HHS Public Access

Author manuscript

Differentiation. Author manuscript; available in PMC 2019 January 01.

Published in final edited form as:

Differentiation. 2018 ; 99: 51–61. doi:10.1016/j.diff.2017.12.003.

The ubiquitin ligase ITCH coordinates small intestinal epithelial homeostasis by modulating cell proliferation, differentiation, and migration

Heather L. Mentrup, **Amanda Hartman**, **Elizabeth L. Thames**, **Wassim A. Basheer**, and **Lydia E. Matesic***

Department of Biological Sciences, University of South Carolina, 715 Sumter St., Columbia, SC 29208, USA

Abstract

Maintenance of the intestinal mucosa is driven by local signals that coordinate epithelial proliferation, differentiation, and turnover in order to separate antigenic luminal contents from the host's immune system. Breaches in this barrier promote gastrointestinal pathologies ranging from inflammatory bowel disease to cancer. The ubiquitin ligase ITCH is known to regulate immune responses, and loss of function of ITCH has been associated with gastrointestinal inflammatory disorders, particularly in the colon. However, the small intestine appears to be spared from this pathology. Here we explored the physiological mechanism that underlies the preservation of mucosal homeostasis in the small intestine in mice lacking ITCH (*Itch*$^{a18H/a18H}$). Histological analysis of the small intestines from young adult mice revealed architectural changes in animals deficient for ITCH, including villus blunting with cell crowding, crypt expansion, and thickening of the muscularis propria relative to age-matched mice sufficient for ITCH. These differences were more prominent in the distal part of the small intestine and were not dependent upon lymphoid cells. Underlying the observed changes in the epithelium were expansion of the Ki67^{+} proliferating transit amplifying progenitor population and increased numbers of terminally differentiated mucus-secreting goblet and anti-microbial producing Paneth cells, which are both important in controlling local inflammation in the small intestine and are known to be dysregulated in inflammatory bowel disease. Homeostasis in the small intestine of *Itch*$^{a18H/a18H}$ animals was maintained by increased cell turnover, including accelerated migration of epithelial cells along the crypt-villus axis and increased apoptosis of epithelial cells at the crypt-villus junction. Consistent with this enhanced turnover, *Itch*$^{a18H/a18H}$ mice carrying the *Min* mutation (*Itch*$^{a18H/a18H}$; *Apc*$^{Min/+}$) displayed a 76% reduction in tumor burden as compared to *Apc*$^{Min/+}$ littermates with normal levels of ITCH. These findings highlight the role of ITCH as an important modulator of intestinal epithelial homeostasis.

*Corresponding author: lmatesic@biol.sc.edu (L.E. Matesic).

Disclosures

None.

Keywords

ITCH; E3 ubiquitin ligase; Intestinal homeostasis; Epithelial differentiation; Cell migration; Colorectal cancer

1. Introduction

In the small intestine, the mucosal epithelium is a folded monolayer of columnar cells that is organized into crypts, which invaginate into the underlying mesenchyme, and villi, which project into the lumen. This structure is ideally suited to provide an essential, physical barrier between the host and its environment that must facilitate the absorption of nutrients while simultaneously preventing the loss of fluids and electrolytes as well as the entry of microorganisms into the body (van der Flier and Clevers, 2009). When the intestinal epithelium is disrupted, commensal and pathogenic microbes gain access to the host organism, prompting an inflammatory response, which can itself cause further tissue damage if not appropriately regulated (Turner, 2009). Thus, communication between mucosal immune cells (particularly those of the myeloid lineage) and the overlying epithelium is essential in maintaining gut homeostasis and in controlling intestinal inflammation (van der Gracht et al., 2016). Preservation of barrier function is dependent, in part, upon the continuous renewal of intestinal epithelial cells (Bischoff et al., 2014). Regeneration of the small intestinal epithelial architecture is a highly complex process that relies on the balanced coordination of cellular proliferation within the crypts of Lieberkühn, preservation of epithelial function through cellular differentiation, and homeostatic cell migration along the crypt-villus axis (Pellettieri and Sanchez Alvarado, 2007). Dysregulation of any one of these aspects of epithelial maintenance can drive a diverse collection of pathologies, ranging from improper nutrient absorption to inflammatory bowel disease (IBD) to intestinal carcinogenesis (Williams et al., 2015).

The rapid and constant renewal of the intestinal epithelium is initiated by the multipotent crypt base columnar (CBC) stem cells that reside at the bottom of the crypts (Barker et al., 2007). Upon cellular division, the CBC stem cells give rise to a rapidly dividing transit-amplifying (TA) population that will commit and differentiate into the five major post-mitotic cells of the small intestinal epithelium (Barker, 2014). The most abundant of these is the absorptive enterocyte. The remaining four post-mitotic cell types originate from the secretory cell lineage and include the mucus-secreting goblet cells, anti-microbial secreting Paneth cells, hormone producing enteroendocrine cells, and tuft cells (Barker, 2014). With the exception of Paneth cells, which migrate deeper into the crypt, the other four post-mitotic cell types normally move onto the villus where they continue to travel upward along this axis, eventually being sloughed off at the tip into the lumen. Because of the rapid turnover of the small intestinal epithelium, both spatial and temporal timing of signals are paramount. Accumulating evidence suggests that post-translational modifications such as ubiquitylation are essential in the regulation of these signals to promote tissue homeostasis (Strikoudis et al., 2014).

Protein ubiquitylation is a highly conserved process characterized by the attachment of a ubiquitin molecule to a lysine residue within a target protein via the sequential action of three enzymatic/scaffolding proteins: the ubiquitin-activating enzyme (E1), the ubiquitin-conjugating enzyme (E2), and the ubiquitin ligase (E3). Ubiquitylation of a target substrate can lead to its degradation in the proteasome or lysosome, to its altered function, or to a change in its subcellular localization (Popovic et al., 2014). The E3 ubiquitin ligase ITCH was originally identified when the molecular etiology of the radiation- and 5-hydroxyurea-induced *a18H* mutation was elucidated, revealing a paracentric inversion on the distal end of mouse chromosome two, the breakpoints of which disrupted both the *Itch* and *Agouti* loci (Perry et al., 1998). Animals homozygous for this null mutation of *Itch* (*Itch*$^{a18H/a18H}$) display lymphoproliferation in the spleen, lymph nodes, and thymus, atopic dermatitis, and pulmonary interstitial inflammation with alveolar proteinosis which culminates in death around 6–8 months of age on a C57BL/6J background (Hustad et al., 1995), whereas animals heterozygous for this mutation appear relatively unaffected with a normal lifespan (Hustad et al., 1995; Parravicini et al., 2008). The skin and lung inflammation in these animals occurs in the absence of known pathogen exposure, implying that immune activation may result from inappropriate inflammatory responses to environmental antigens at mucosal surfaces. Consistent with this assertion, loss of ITCH function has also been associated with a gastrointestinal inflammatory phenotype in both mice and humans (Kathania et al., 2016; Lohr et al., 2010; Ramon et al., 2011; Tao et al., 2009). In mice, this appears to be more severe in the colon with moribund *Itch*$^{a18H/a18H}$ mice developing spontaneous colitis characterized by an increase in mixed inflammatory infiltrate and colonic epithelial destruction that was not observed in their age- and gender-matched wild type counterparts and has been hypothesized to be lymphoid-driven (Kathania et al., 2016). However, only mild inflammation has been observed in the small intestine of similarly aged (*i.e.*, 5–7 month old) animals lacking ITCH (Kathania et al., 2016; Ramon et al., 2011). This led us to hypothesize that, owing to differences in architecture, function, and microbiota composition, additional compensatory pathways may be activated in animals lacking ITCH in order to better maintain homeostasis in the small intestine as compared to what has already been described for the colon. Using the previously characterized *Itch*$^{a18H/a18H}$ mouse model, we found that, in the distal small intestines of *Itch*$^{a18H/a18H}$ animals, there were increased numbers of goblet and Paneth cells which correlated with increased proliferation of progenitor cells and expansion of the crypts. However, overall, homeostasis and cell number was maintained in these animals by accelerated migration and increased apoptosis of epithelial cells as compared to wild type animals. Furthermore, these changes in epithelial cell dynamics were associated with a 76% reduction in small intestinal tumor burden in animals lacking *Itch* expression on an *Apc*$^{Min/+}$ background as compared to ITCH-sufficient *Apc*$^{Min/+}$ littermates. Collectively, these data demonstrate a previously unappreciated role for ITCH in the regulation of intestinal epithelial homeostasis, and provide further insight into regional differences in this process along the intestines.

2. Materials and methods

2.1. Animals

Animals homozygous for a null allele of *Itch* (*Itch*$^{a18H/a18H}$) have been previously described (Hustad et al., 1995). For this line, the *a*^{18H} allele was backcrossed to C57BL/6J for 27 generations. Therefore, age-matched male and female C57BL/6J mice were used as referent controls (*Itch*$^{+/+}$) in the indicated experiments. To study the effect of this mutation on APC-induced tumorigenesis, a two generation intercross was performed. Specifically, *Itch*$^{a18H/a18H}$ mice were bred to *Apc*$^{Min/+}$ animals (JAX stock #002020) to produce *Itch*$^{a18H/+}$; *Apc*$^{Min/+}$ and *Itch*$^{a18H/+}$; *Apc*$^{+/+}$ offspring, which were interbred to generate *Itch*$^{+/+}$; *Apc*$^{+/+}$, *Itch*$^{a18H/a18H}$; *Apc*$^{+/+}$, *Itch*$^{a18H/a18H}$; *Apc*$^{Min/+}$, and *Itch*$^{+/+}$; *Apc*$^{Min/+}$ animals for analysis. For all experiments, both genders were represented in each genotype in all experiments. The specifics of this (as well as numbers of litters represented in each cohort) is summarized in Supplemental Table 1. All experiments were conducted in full compliance with the Institutional Animal Care and Use Committee of the University of South Carolina.

2.2. Histology and staining

Small intestines derived from young adult animals were flushed with phosphate-buffered saline (PBS) after being cut into three equally sized segments (designated proximal, middle and distal), opened longitudinally, and fixed overnight with either 4% paraformaldehyde or with 10% neutral buffered formalin. Swiss-rolled intestinal tissues or were paraffin-embedded and sectioned at 5 μm. Hematoxylin and eosin (H & E) staining was performed to assess tissue morphology. Alcian blue and nuclear fast red staining was performed by applying alcian blue, pH 2.5 for 30 min at 25 °C followed by 0.1% nuclear fast red for 5 min. The Grimelius stain was performed according to previously published methodology (Grimelius, 2004). Briefly, tissue sections were treated with a 0.03% silver nitrate staining solution (Fisher Scientific, S181) for 3 h at 60 °C followed by a 2 min treatment with a silver reducing solution (5% Sodium Sulfite/1% Hydroquione) that was pre-warmed to 58 °C. Alkaline phosphatase (AP) staining was carried as previously described (Burstone, 1961). Specifically, a 2% naphthol AS-MX phosphate solution diluted in N,N-dimethyformamide was added to a 50%/50% mixture of Tris buffer, pH 8.74 and distilled water to create a final solution containing 0.5% napththol AS-MX phosphate in Tris buffer. This was then filtered through a 0.45 μm filter. Slides were placed in the solution for 45 min at 37 °C and washed before counter-staining with hematoxylin.

2.3. Immunohistochemistry and Immunofluorescence

For immunohistochemistry (IHC), antigen unmasking was performed using target retrieval solution for Ki67 (Dako # S1699) or 10 mM Tris–HCl/1 mM ethylenediaminetetraacetic acid (EDTA), pH = 9 for 30 min at 95 °C for cleaved-caspase 3. Sections were blocked in a solution containing 10% normal goat serum, 2% bovine serum albumin, and 0.2% Triton X-100 in Tris buffered saline (10 mM Tris–HCl, pH 7.6, 150 mM NaCl). An additional hydrogen peroxidase block was performed for 20 min at 25 °C. The primary antibodies recognizing either Ki67 (B56, BD Pharmingen, 1:100) or cleaved-caspase 3 (Cell Signaling Technology, #9664, 1:100) were diluted in Tris buffered saline containing 1% normal goat serum and 0.1% Triton X-100 and incubated on sections in a humidified chamber overnight

at 4 °C. The antibody was visualized using the EnVision+ system-HRP per the manufacturer's instructions (Dako # K4006). Brightfield images were acquired on a Zeiss Axio Imager A1 equipped with an AxioCam MRc5 camera.

Tissue immunofluorescence for lysozyme was performed as previously described (Basheer et al., 2015) with the following modifications: 5 μm paraffin sections were blocked for 1 h before applying an anti-lysozyme antibody (RP028, Diagnostic BioSystems, 1:100) overnight at 4 °C. AlexaFluor659-conjugated goat anti-rabbit secondary (Jackson ImmunoResearch) was applied at a 1:500 dilution for 1 h before mounting sections in Fluoro-gel II with DAPI (17985-51, Electron Microscopy Sciences). Phase contrast-coupled fluorescent images were acquired on a Leica DMI6000B epifluorescence microscope equipped with a Hamamatsu ORCA-R^2 CCD camera.

2.4. Quantitative measurements: histological measurements, cell proliferation, and post-mitotic cell differentiation

All parameters quantified by histological examination were assessed in the distal segment from four or five 8–10 week old animals of each genotype (*i.e.*, $Itch^{+/+}$, n = 4 or 5 and $Itch^{a18H/a18H}$, n = 4 or 5). Crypt and villus areas were quantified using a minimum of 25 well-oriented crypt or villus structures from at least seven different 10x fields per animal. The crypt or villus unit was outlined using the polygon tool in ImageJ, and the areas were quantified in μm^2. Cell proliferation was measured by first manually counting the total number of $Ki67^+$ cells stained by IHC in 25 well-oriented crypts from a minimum of nine 20x fields per animal. Then, the total number of cells in those same crypts was determined by enumerating the nuclei stained with Ki67 and/or hematoxylin. To calculate the average percentage of $Ki67^+$ cells in a crypt, the number of $Ki67^+$ cells was normalized to total cell number for that crypt and expressed as a percentage.

Phase contrast-coupled fluorescence images immunostained with an anti-lysozyme antibody were used to determine average Paneth cell number. In particular, individual Paneth cells were delineated using the cell membrane highlighted by phase-contrast microscopy, the DAPI-stained nucleus, as well as reactivity with the anti-lysozyme antibody. Paneth cells were counted in 30 crypts from a minimum of twelve 20x fields per animal. Average goblet cell and enterocyte number was determined by staining sections with alcian blue and a nuclear fast red counterstain. Goblet cells were recognized on the basis of the reactivity of their cytoplasm with alcian blue and by their characteristic shape, while enterocytes were not reactive with alcian blue and were instead identified by their typical columnar appearance. Both types of cells were counted on 30 villi in at least eight different 10x fields per animal. Similarly, enteroendocrine cells identified through Grimelius stain were counted from 30 villi in eight different 10x fields per animal.

2.5. Bromodeoxyuridine (BrdU) migration assay

Twelve young adult $Itch^{+/+}$ and twelve young adult $Itch^{a18H/a18H}$ animals were intraperitoneally injected with 100 mg/kg BrdU (B5002, Sigma) dissolved in sterile PBS. Three animals of each genotype were randomly assigned to one of three cohorts and euthanized at 2, 24, 48, or 72 h post-injection. The small intestines from these animals were

cut into equally sized proximal, middle, and distal segments and flushed with PBS prior to 4% paraformaldehyde fixation, paraffin-embedding, and sectioning at 5 μm. IHC was performed as described above using anti-BrdU (3D4, BD Pharmingen, 1:8000). Images were acquired by bright field microscopy on a Zeiss Axio Imager A1 equipped with an AxioCam MRc5 camera and subsequently analyzed using ImageJ to determine migration and villus lengths. Percent cell migration was assessed from 25 villi in at least five different 10x fields per animal and calculated by normalizing the length of the furthest migrated epithelial BrdU^{+} cell from the base of the villus to the entire length of the villus from BrdU immunostained sections and converting to a percentage.

For figure presentation, brightfield images of sections immunostained with an anti-BrdU antibody were transformed to a spectral image using ImageJ. This was accomplished by first inverting the images and then converting them to 8-bit gray scale. In order to specifically highlight cells that had taken up the BrdU label, the pixel intensity for those nuclei staining only for hematoxylin was subtracted out by calculating their background values. Specifically, for each converted image, a minimum of six different BrdU^{-} nuclei were identified throughout the image and the pixel value for each was determined using a constant, ImageJ pre-defined area for the cursor. These values were averaged and considered the background level for each image. A similar background level was calculated in all the images except the 72 h *Itch*$^{a18H/a18H}$ image, which was higher. To account for this discrepancy, 55 pixels were subtracted from all the images except the 72 h image captured from the *Itch*$^{a18H/a18H}$ animal in which 67 pixels were subtracted due to high background. Finally, the royal lookup table was applied to all images to re-colorize them.

2.6. Transmission electron microscopy

The small intestine from four young adult animals of each genotype was cut into three equally sized segments, flushed with PBS, and then opened longitudinally. The proximal segment was dissected into 4 mm^2 pieces which were fixed in 2% glutaraldehyde/2% paraformaldehyde and secondarily post-fixed in buffered 1% osmium tetroxide/1.5% potassium ferricyanide. After dehydrating in ethanol, the samples were infiltrated and embedded in PolyBed 812 epoxy and allowed to polymerize for at least 48 h at 60 °C. At that time, blocks were sectioned at approximately 90 nm on a Leica UltraCut R and post stained with 2% uranyl acetate (aq) and Hanaichi's calcined lead citrate. Images were obtained on a JEM 1400+ with an AMT mid-mount camera.

2.7. Polyp counts

The small intestines from 15 week-old male and female *Itch*$^{+/+}$; *Apc*$^{+/+}$, *Itch*$^{a18H/a18H}$; *Apc*$^{+/+}$, *Itch*$^{a18H/a18H}$; *Apc*$^{Min/+}$, and *Itch*$^{+/+}$; *Apc*$^{Min/+}$ animals were cut into 4 equally sized segments, flushed with PBS, opened longitudinally, and fixed overnight in 10% neutral buffered formalin. The samples were stained with 0.1% methylene blue to identify tumors. Total tumor number for each animal was assessed by counting and tabulating the polyp number along the entire axis of the small intestine by an observer blinded to genotypes.

2.8. Statistics

Statistical comparisons of $Ki67^+$ cells, Paneth cells, goblet cells, enteroendocrine cells, enterocytes, BrdU migration, and tumor counts (reported as mean and standard deviation (SD) or standard error of the mean (SEM), as indicated, 2-tailed unpaired *t*-test for mean comparisons, Mann-Whitney test for comparing non-parametric medians of non-normally distributed enteroendocrine cells, and one-way ANOVA with a *post hoc* Tukey correction for tumor counts) were performed in Microsoft Excel or Prism Software (GraphPad Software, Inc) and plotted using Prism software. A p-value < 0.05 was considered statistically significant.

3. Results

3.1. $Itch^{a18H/a18H}$ animals have altered small intestinal morphology

Using a previously described loss of function mouse model (Hustad et al., 1995), the role of ITCH in intestinal homeostasis was examined by first characterizing the impact that loss of ITCH has on the morphology of the small intestines in young adult animals. This was accomplished by harvesting the small intestines from four or five 8–10 week old mice of each genotype and separately examining the architecture of the proximal, middle, and distal thirds of the intestine to account for known regional variations in structure. Interestingly, examination of H & E stained sections from the various segments revealed hyperplasia of the crypts which became more prominent caudally along the small intestinal tract of $Itch^{a18H/a18H}$ animals as compared to ITCH sufficient referent controls (Fig. 1A). Additionally, villus blunting (with more disorganized epithelial cell organization) as well as thickening of the muscularis propria were observed in the distal portion of animals lacking ITCH (asterisk, Fig. 1A) and was associated with occasional mild mucosal inflammation (arrow, Fig. 1A). These phenotypes were also noted in $Itch^{a18H/a18H}; Rag1^{-/-}$ animals which lack functional lymphoid cells (Fig. S1 and (Tao et al., 2009)), indicating that these changes were dependent on cues garnered from epithelial and/or innate immune cells. To quantify the changes in size of the crypts and villi in $Itch^{a18H/a18H}$ animals, we measured the area of 25 crypts and 25 villi from $Itch^{+/+}$ and $Itch^{a18H/a18H}$ animals in each region of the small intestine. Consistent with the apparent crypt expansion noted microscopically, the crypt area was significantly increased in the middle and distal segments of $Itch^{a18H/a18H}$ intestine as compared to age-matched wild type animals (19,772.23 μm^2 vs 11,165.53.12 μm^2 and 22,653.25 μm^2 vs. 15,780.51 μm^2, respectively) as determined by 2-tailed, unpaired *t*-test (Fig. 1B). While there was a trend toward increased villus area across the entire small intestine, only in the distal segment was a statistically significant increase noted in animals lacking ITCH relative to those that were sufficient for ITCH (62,056.18 μm^2 vs. 47,144.47 μm^2, Fig. 1C). Therefore, for our subsequent analyses, we focused on changes in the distal segment of the small intestine.

3.2. Expansion of the crypt in adult $Itch^{a18H/a18H}$ animals is associated with an increase in the number of proliferating cells and Paneth cells in the distal small intestine

As there was a statistically significant increase in the crypt area of $Itch^{a18H/a18H}$ animals relative to $Itch^{+/+}$ controls, we hypothesized that an increase in cell number might underlie this expansion. Indeed, when the total number of cells in the crypts was calculated in tissues

derived from five young adult animals of each genotype, a statistically significant increase in cell number was found in animals lacking ITCH (Fig. S2). To determine which cell populations might be expanded in the crypt, we first performed IHC using an antibody that recognizes the proliferation marker Ki67 since crypts are mostly composed of rapidly proliferating progenitor TA cells (Fig. 2A). Upon evaluation of 25 well-oriented crypts from a minimum of nine 20x fields per animal (n = 5 for each genotype), 40.14 ± 4.91 (SD) $Ki67^+$ cells on average were found in the crypts of the $Itch^{a18H/a18H}$ animals whereas 29.056 ± 2.91 (SD) $Ki67^+$ cells on average were found in the crypts of $Itch^{+/+}$ controls, and this difference was found to be statistically significant by 2-tailed, unpaired student *t*-test (Fig. 2B). Although there was an increase in the absolute number of $Ki67^+$ cells detected in $Itch^{a18H/a18H}$ animals, there was no difference in the percentage of proliferating cells within the crypt when compared to $Itch^{+/+}$ controls (Fig. 2B), suggesting that progenitors cells were not the only cell type contributing to this increase in total cell number within the crypt.

In addition to stem and progenitor cells, Paneth cells also reside in the crypt. To test whether increased numbers of Paneth cells might be contributing to the increased crypt area observed in $Itch^{a18H/a18H}$ mice, small intestinal sections from five animals of each genotype were immunostained with an antibody recognizing lysozyme, a mature Paneth cell maker (Fig. 2C), allowing for the enumeration of Paneth cells in 30 crypts from a minimum of twelve 20x fields per animal. Interestingly, there was a significant increase in Paneth cells in the crypts of $Itch^{a18H/a18H}$ animals (6.82 ± 0.64, SEM) compared to $Itch^{+/+}$ controls (5.17 ± 0.19, SEM). When the means were compared by unpaired, 2-tailed student *t*-test, the difference was found to be statistically significant (Fig. 2D). Taken together, these results indicate that increases in the number of proliferating progenitor cells and differentiated Paneth cells contributed to the crypt expansion observed in $Itch^{a18H/a18H}$ animals.

3.3. $Itch^{a18H/a18H}$ animals have increased numbers of goblet cells along the villi of the distal small intestine

The epithelium of the small intestine is comprised of a variety of different cell types that arise from the rapidly dividing TA progenitor population found within the crypt. Since there was an expansion of proliferating cells in the crypts of mice lacking ITCH and since Paneth cells are only one of several different kinds of differentiated cells contributing to the epithelial architecture of the small intestine, it was a distinct possibility that other classes of post-mitotic cells which localize to the villi could also be altered in $Itch^{a18H/a18H}$ animals. To determine if goblet and enteroendocrine cells were also affected in $Itch^{a18H/a18H}$ animals, we stained small intestinal tissue sections obtained from four animals of each genotype to specifically highlight each type of post-mitotic secretory cell. In particular, goblet cells were visualized using alcian blue, a stain identifying glycosylated mucins (Fig. 3A), and the cell number determined by counting positively stained cells on 25 villi in at least eight different 10x fields per animal. Interestingly, there was a 48% increase in the number of goblet cells on the villus of $Itch^{a18H/a18H}$ animals as compared to $Itch^{+/+}$ animals (10.93 ± 0.98 (SEM) vs. 7.37 ± 0.69 (SEM)), and this difference was statistically significant by 2-tailed, unpaired *t*-test (Fig. 3D). However, no statistically significant difference in the number of enteroendocrine cells (visualized by Grimelius stain, which reacts with the hormones in the secretory granules, and quantified in 30 villi from eight different 10x fields per animal) was

observed in the distal small intestine derived from *Itch*$^{a18H/a18H}$ mice as compared to those derived from age-matched ITCH sufficient controls. Because of the left-shifted distribution of enteroendocrine cells in animals of both genotypes, a Mann-Whitney comparison of non-parametric medians was performed to determine significance for this population (Figs. 3B and 3D).

In addition to the post-mitotic cells derived from the secretory lineage, the absorptive enterocyte (the most abundant cell type in the small intestine) is essential to the structure and function of the small intestine. For this reason, mature enterocytes were characterized by staining distal intestinal tissues derived from young adult mice of both genotypes with AP in order to visualize the brush boarder (which is critical in nutrient absorption). When examining the sections of *Itch*$^{+/+}$ and *Itch*$^{a18H/a18H}$-derived tissues, no appreciable difference in AP staining was seen, suggesting that the overall architecture and functionality of the enterocytes was preserved even in the absence of ITCH (Fig. 3C). To determine whether there was instead a difference in enterocyte number between the two genotypes, the number of enter-ocytes was determined using alcian blue/nuclear fast red stained distal intestinal sections from four animals of each genotype. For this analysis, enterocytes were identified on the basis of their nuclear morphology and typical columnar cell profile and were counted from 25 villi in at least eight different 10x fields per animal. Although there was a trend towards reduced enterocyte number in the ileum of *Itch*$^{a18H/a18H}$ animals (48.52 ± 2.38, SEM) as compared to the control (54.67 ± 3.13, SEM, Fig. 3D), this difference was not statistically significant by two-tailed unpaired *t*-test ($p = 0.07$). Additionally, there was no statistically significant difference between genotypes in the total number of epithelial cells on those same villi (Fig. S3). Collectively, these data suggest that proliferating progenitor cells in the *Itch*$^{a18H/a18H}$ animals still retain the ability to give rise to both the absorptive and secretory cell lineage, albeit the percentage of the cell types are altered.

3.4. Itch$^{a18H/a18H}$ animals have increased epithelial cell turnover

Because *Itch*$^{a18H/a18H}$ animals have an increase in the number of proliferating progenitor cells within the crypt compartment yet still have comparable numbers of post-mitotic cells on the villus as age-matched ITCH sufficient controls, we speculated that animals lacking ITCH might have increased apoptosis of epithelial cells. To evaluate steady-state apoptosis levels, IHC was performed on sections derived from the distal small intestines of four young adult animals of each genotype using an antibody that recognizes cleaved-caspase 3, a critical executioner for apoptosis. As would be expected under normal conditions, very few apoptotic cells could be detected in *Itch*$^{+/+}$ intestines, except for the rare epithelial cell at the tip of a villus that was presumably in the process of being sloughed off (Fig. 4). In addition to the occasional cleaved-caspase 3^+ cell at the tip of a villus, there were a number of apoptotic cells at the crypt-villus junction in *Itch*$^{a18H/a18H}$ animals that were never seen in the intestines derived from *Itch*$^{+/+}$ mice (second row of images, Fig. 4). Thus, there was increased apoptosis of epithelial cells in the distal small intestines derived from animals lacking ITCH, even without some sort of stress or stimulus.

Another potential mechanism for more rapid turnover of the epithelium includes enhanced homeostatic epithelial cell migration along the crypt-villus axis, particularly since this is

known to be influenced by proliferation within in the small intestinal crypt, wherein an increase or reduction in cell proliferation can enhance or slow migration, respectively (Parker et al., 2017). Given the observed increase of proliferative cells within the crypts of *Itch*$^{a18H/a18H}$ animals, we sought to evaluate intestinal epithelial cell migration by intraperitoneally injecting twelve young adult *Itch*$^{a18H/a18H}$ and twelve young adult *Itch*$^{+/+}$ animals with 100 mg/kg BrdU, and three animals of each genotype were euthanized 2, 24, 48 or 72 h post injection. IHC was performed on sections from the distal small intestines of these animals using an anti-BrdU antibody in order to localize the cells that had taken up the BrdU pulse. As illustrated in Fig. 5A, at 2 h, all labeled cells were contained within the crypts of both ITCH sufficient and ITCH deficient mice. By 24 h following injection, there were distinct differences between the two genotypes. In particular, mice lacking ITCH showed accelerated exodus of the label from the proliferating cells in the crypt at 24 h, increased migration up the villus at 48 h, and nearly complete elimination by 72 h. To quantify the difference in cell migration along the villus while simultaneously accounting for the influence of ITCH on the crypt-villus architecture, a normalized measure of cell migration was calculated by dividing the measured length of the furthest migrated BrdU^{+} cell on the villus to the entire length of the villus from 25 well-oriented villi in at least five different 10x fields per animal and expressed as a percentage (Fig. 5B). Consistent with our qualitative observations, cell migration in the *Itch*$^{a18H/a18H}$ animals was more than double that of the *Itch*$^{+/+}$ animals at the 24 h time point (33.46 ± 3.64%, SD, vs. 15.47 ± 4.68%, SD), which was statistically significant. A similar trend was apparent at both the 48 and 72 h time points, though the difference between genotypes was not as drastic due to the sloughing of cells from the villus tip. In particular, at 48 h, the edge of the BrdU label front had migrated 58.57 ± 1.91% (SD) up the villus in *Itch*$^{a18H/a18H}$ animals whereas, on average, in *Itch*$^{+/+}$ animals, the leading edge had not yet reached the midway point (47.15 ± 2.02%, SD). At 72 h post injection, the BrdU pulse was nearly completely shed in animals lacking ITCH, and those labeled cells that remained were at the very tip of the villi (97.58 ± 0.09%, SD). In contrast, in those animals sufficient for ITCH, the vast majority of the labeled cells were present with the farthest migration point being 90.39 ± 4.36% the length of the villus. Collectively, our data suggest that expansion of the proliferating progenitor cell population leads to accelerated cell migration along the crypt-villus axis in *Itch*$^{a18H/a18H}$ animals.

In the small intestine, the intercellular junctions of epithelial cells have been noted to be highly dynamic in order to accommodate the rapidly dividing cells while still maintaining tissue integrity (Peglion et al., 2014). Further, alterations in adherens junctions and desmosomes are known to influence cell migration in the small intestine (Schneider et al., 2010). Since *Itch*$^{a18H/a18H}$ animals have increased proliferation and cell migration compared to *Itch*$^{+/+}$ animals, we hypothesized the cell-cell junctions might be affected in mice lacking ITCH. To test this hypothesis, small intestinal tissues derived from four young adult *Itch*$^{a18H/a18H}$ and four age-matched *Itch*$^{+/+}$ mice were examined by transmission electron microscopy. This analysis revealed several differences in the ultrastructure of these junctions. In particular, while tight junctions could be readily identified in both *Itch*$^{a18H/a18H}$ and *Itch*$^{+/+}$ derived tissue (Fig. 6, asterisks), adherens junctions were less discernable in small intestines derived from *Itch*$^{a18H/a18H}$ animals (Fig. 6, arrow) and the associated actin cytoskeleton appeared to be less organized. In addition, there was a complete absence of

desmosomes in the small intestines of *Itch*$^{a18H/a18H}$ mice (Fig. 6, arrow head). Collectively, these data are consistent with a role for ITCH in regulating intestinal epithelial turnover.

3.5. Loss of ITCH significantly decreases intestinal adenoma formation in the small intestine of Apc$^{Min/+}$ animals

As the epithelium of the small intestine is under rapid and continuous renewal, stringent regulation of epithelial cell turnover is essential to prevent the growth of intestinal adenomas (Wong et al., 1996). In fact, increases in homeostatic cell migration have been associated with reduced *Apc*$^{Min/+}$ -induced tumorigenesis in the small intestine (Sansom et al., 2007). Since *Itch*$^{a18H/a18H}$ animals have enhanced epithelial cell migration, we hypothesized that loss of ITCH would decrease intestinal adenoma formation. To test this hypothesis, the *Min* mutation (*Apc*$^{Min/+}$) was moved onto the *Itch*$^{a18H/a18H}$ background via a two generation intercross. This allowed for polyp assessment in *Itch*$^{+/+}$; *Apc*$^{+/+}$ (ITCH and APC sufficient), *Itch*$^{a18H/a18H}$; *Apc*$^{+/+}$ (ITCH deficient but APC sufficient), *Itch*$^{a18H/a18H}$; *Apc*$^{Min/+}$ (ITCH deficient and carrying the mutant *Apc* allele), and *Itch*$^{+/+}$; *Apc*$^{Min/+}$ (ITCH sufficient and carrying the mutant *Apc* allele) littermates. Total polyp number in the small intestines derived from eleven animals of each genotype (with approximately equal numbers of males and females) was determined when the animals reached 15 weeks of age. Consistent with previous reports (Tucker et al., 2002, 2005), a total of 115.7 ± 52.49 (SD) polyps were observed in *Itch*$^{+/+}$; *Apc*$^{Min/+}$ animals at this age (Fig. 7). Interestingly, the *Itch*$^{a18H/a18H}$; *Apc*$^{Min/+}$ animals examined had only 27.36 ± 19.62 (SD) polyps (Fig. 7). This represents a 76% reduction in tumor burden as compared to the *Itch*$^{+/+}$;*Apc*$^{Min/+}$ cohort, which was statistically significant ($p < 0.001$). However, the number of polyps found in *Itch*$^{a18H/a18H}$; *Apc*$^{Min/+}$ animals was not statistically different from that of either wild-type animals (*Itch* $^{+/+}$; *Apc*$^{+/+}$) or from animals lacking ITCH (*Itch*$^{a18H/a18H}$; *Apc*$^{+/+}$) as assessed by one-way ANOVA with *post hoc* Tukey correction. Further, despite the altered cell-cell junctions seen in mice lacking ITCH (Fig. 6), this accelerated migration appeared to be physiological and was not associated with a pathological epithelial-to-mesenchymal transition (EMT) process as EMT markers N-cadherin and vimentin could not be detected by western blot on villus protein extracts from either *Itch*$^{+/+}$ or *Itch*$^{a18H/a18H}$ animals but were detected in positive controls (heart tissue lysate for N-cadherin and HeLa lysate for vimentin, Fig. S4). Thus, as a whole, these data suggest increased cell turnover in *Itch*$^{a18H/a18H}$ mice protects from the initiation of small intestinal adenoma formation in *Apc*$^{Min/+}$ animals.

4. Discussion

As a dividing line between self and non-self, the mucosal surface of the intestine is essential to maintaining homeostasis, and its breach is associated with pathologies like IBD (Mankertz and Schulzke, 2007), chronic viral infections (Brenchley et al., 2006; Sandler et al., 2011), and extra-intestinal autoimmune diseases such as type 1 diabetes (Wen et al., 2008), rheumatoid arthritis (Wu et al., 2010), and multiple sclerosis (Berer et al., 2011; Lee et al., 2011). However, the intestine is far from being a single homogeneous organ; rather, it consists of a number of anatomically and functionally specialized segments, each with distinct environmental pressures (Agace and McCoy, 2017). Here, we have identified a novel role for the E3 ubiquitin ligase ITCH in the proliferation, migration, and differentiation of

small intestinal epithelial cells, and, in so doing, offer a putative physiological mechanism for the attenuated inflammatory phenotype in the small intestine versus what has been previously reported in the large intestine of animals lacking ITCH (Kathania et al., 2016; Ramon et al., 2011). Consistent with those studies, we found little inflammation in the mucosa of the small intestine of young adult *Itch*$^{a18H/a18H}$ mice despite the chronic inflammation that is known to accumulate with age at other mucosal surfaces like the lungs and skin (Hustad et al., 1995). Even though there was a lack of inflammatory infiltrate, distinct architectural changes (including villus blunting with some cellular disarray, crypt expansion, and thickening of the muscularis propria) were present along the length of the small intestine, and these were most pronounced in the distal portion. Many of these same alterations were seen in the small intestines of *Itch*$^{a18H/a18H}$; *Rag1*$^{-/-}$ mice which lack a functional lymphoid compartment of the immune system. This suggests that these changes result from altered programs in non-hematopoietic cells, in the resident innate immune cells, or a combination thereof.

Animals lacking ITCH also displayed increased numbers of Paneth and goblet cells in the distal small intestine. Paneth cells are normally only found in the small intestinal epithelium and play an important protective role in intestinal homeostasis by secreting antimicrobial peptides (Mukherjee et al., 2008; Vaishnava et al., 2008). Further, defects in Paneth cell function have been described in IBD patients (Elphick and Mahida, 2005; Wehkamp et al., 2008) as well as in a number of mouse lines that develop spontaneous intestinal inflammation including *Casp8*$^{IEC\text{-}KO}$ (Gunther et al., 2011), *FADD*$^{IEC\text{-}KO}$ (Welz et al., 2011), *NEMO*$^{IEC\text{-}KO}$ (Nenci et al., 2007), and *IKK2ca*$^{IEC\text{-}KO}$ (Vlantis et al., 2011). While the phenotypes in these lines result from intestinal epithelial-specific loss of proteins, the effects of Paneth cell function are far from cell autonomous as they help shape the microbiome, modulate the mucosal immune response, and provide important signaling cues in the intestinal stem cell niche (Okumura and Takeda, 2017). Similarly, the mucins secreted by goblet cells in the small and large intestine offer a protective barrier against commensal and pathogenic bacterial contact with the immune system. However, the composition of the mucous layer is different in the small and large intestine. In the former, there is a loose, more porous mucus that better facilitates the absorption of nutrients and depends on peristaltic actions to propel trapped microbes down the digestive tract whereas in the large intestine, the mucus is made of two discrete layers (an upper, thinner layer and a thicker lower layer) that has more permanence and thus more resident bacteria (Johansson and Hansson, 2016). As with defects in Paneth cell function, goblet cell depletion or dysfunction is a frequent histopathological feature of IBD (Gersemann et al., 2009). Thus, increased numbers of goblet and Paneth cells in the small intestine of animals lacking ITCH may protect it from the more severe inflammation observed in the colon.

In *Itch*$^{a18H/}$a18H mice, increased numbers of Paneth and goblet cells were associated with increased proliferation of progenitor cells in the crypt. It is tempting to speculate that either cell intrinsic or local cues promote secretory cell specification towards these cells fates. Differentiation within the secretory cell lineage is highly complex wherein a heterogeneous population of precursors exists to direct lineage specification toward enteroendocrine cells or a common goblet and Paneth progenitor cell (Basak et al., 2014). While loss of ITCH was associated with an increase in goblet and Paneth cell numbers, enteroendocrine lineage

specification and maturation appeared unaffected since there were equivalent numbers of these cells in the distal small intestine of mice sufficient and deficient for ITCH (Fig. 3). Thus, ITCH may influence goblet and Paneth cell differentiation downstream of this specification step, potentially through the regulation of transcription factors such as SPDEF (Gregorieff et al., 2009).

While changes in epithelial differentiation might be driven by epithelial-intrinsic factors, it is also a formal possibility that they result secondarily from signals from the surrounding stroma. In fact, both mesenchymal and immune cells that normally reside in the lamina propria also contribute to intestinal self-renewal. Secretion of Hedgehog (Hh) ligands from the epithelium activates this signaling pathway within the mesenchyme, which, in turn, can influence intestinal homeostasis by altering cell proliferation, differentiation, inflammation, and turnover (Buller et al., 2012; Powell et al., 2011). Interestingly, ITCH has also been shown to negativity influence Hh signaling by targeting the downstream transcription factor GLI1 (Di Marcotullio et al., 2011), but it remains to be determined how loss of ITCH might impact Hh signals in the mesenchyme and innate immune system. In addition to their capacity as potential targets for Hh signals, inflammatory cells within the lamina propria can influence epithelial homeostasis via the release of proinflammatory cytokines that are capable of feeding back onto the intestinal epithelium to modulate renewal (Garrett et al., 2010). Interestingly, ITCH deficient animals have an increase in the mucosal production (particularly in the colon) of the proinflammatory cytokines TNF-α, IL-1β, IL-6, and IL-17 (Kathania et al., 2016; Tao et al., 2009; Theivanthiran et al., 2015), which are similarly dysregulated during gastrointestinal inflammation and barrier dysfunction (Schenk and Mueller, 2008). In order to pinpoint the initiating signals for the altered intestinal homeostasis observed in ITCH deficient mice, future studies employing the recently generated floxed allele of *Itch* (Jin et al., 2013) are necessary to delineate the tissue-specific contribution of ITCH in the epithelium, immune system, and mesenchyme in isolation from the other genes potentially influenced by the a^{18H} inversion to gain important additional insight into the multifaceted role ITCH plays in mucosal barrier function.

Increased proliferation in the small intestinal crypts of animals lacking ITCH was balanced by increased apoptosis at the crypt-villus junction and by the enhanced migration and shedding of epithelial cells. Renewal of the small intestinal epithelium is very rapid, and complete epithelial turnover occurs every 4–5 days (van der Flier and Clevers, 2009). Turnover in $Itch^{a18H/a18H}$ animals is accelerated even further, with approximately 98% of cells being shed from the villus after 3 days (Fig. 5). This increased migration correlated with the presence of altered cell-cell junctions between intestinal epithelial cells. In particular, ITCH deficient mice lacked desmosomes and had disorganized adherens junctions while the tight junctions appeared to remain intact. Interestingly, E-cadherin, a critical component of adherens junctions, has been shown to influence intestinal homeostasis. Its loss in the intestinal epithelium was associated with altered differentiation and maturation of Paneth and goblet cells, induction of cell death, loss of adherens junctions and desmosomes, and mislocalization of Paneth cells along the crypt-villus axis of the small intestine, and this phenotype was more severe in the colonic epithelium despite the fact that more residual E-cadherin expression was retained there (Schneider et al., 2010). Further, overexpression of E-cadherin within the intestinal epithelium resulted in suppression of

proliferation and a reduction in migration along the crypt-villus axis (Hermiston et al., 1996). As mice lacking ITCH still have adherens junctions (albeit disorganized ones), it is possible that there might be a slight decrease in E-cadherin within epithelial cells that is sufficient to contribute to increased proliferation, accelerated migration, and increased apoptosis of epithelial cells within the small intestine which does not affect maturation programs. Because of the reported disparity in response to loss of E-cadherin between the epithelium of the small intestine and that of the colon, it is tempting to speculate that this might contribute to the different inflammatory profiles of the small and large intestine in *Itch*$^{a18H/a18H}$ mice.

Further evidence that homeostasis is more appropriately regulated in the small intestine than in the colon of mice lacking ITCH comes from our observation that *Itch*$^{a18H/a18H}$; *Apc*$^{Min/+}$ animals had a 76% reduced tumor load as compared to *Itch*$^{+/+}$; *Apc*$^{Min/+}$ littermates (Fig. 7), whereas ITCH deficient mice have been reported to be more susceptible to the induction of colitis-associated cancer which develops in the context of chronic inflammation of the colon (Kathania et al., 2016). This likely reflects, in part, the different initiating events in these types of tumors. Specifically, while the *Apc*$^{Min/+}$ mouse more closely parallels what occurs in sporadic colon cancers where there is a sequential accumulation of genetic mutations that promotes a progressively more malignant phenotype in what has been dubbed the "adenoma-carcinoma sequence" (Cho and Vogelstein, 1992), colitis associated cancer is driven by the activation of completely different pathways, usually without constitutive activation of the APC-β-catenin-TCF axis (Foersch and Neurath, 2014). Furthermore, the increased cell turnover in the small intestine of ITCH deficient animals potentially contributes to the decrease in adenoma initiation observed in *Itch*$^{a18H/a18H}$; *Apc*$^{Min/+}$ mice. Previous studies have shown that increased homeostatic epithelial migration was associated with reduced *Apc*$^{Min/+}$ -induced tumorigenesis in the small intestine (Sansom et al., 2007), suggesting that perturbations in the intestinal epithelial cell migration observed in *Itch*$^{a18H/a18H}$ mice could influence intestinal adenoma formation by limiting the anchorage of cancer-initiating cells needed for adenoma induction and growth. However, there was no evidence that animals lacking ITCH had a switch from E-cadherin to N-cadherin expression which is observed in EMT and promotes the invasive capabilities of cancer cells (Halbleib and Nelson, 2006), though this possibility needs to be more thoroughly evaluated in a more aggressive colorectal cancer model than the *Apc*$^{Min/+}$ mouse because the tumors in those animals rarely become invasive (Nalbantoglu et al., 2016).

In conclusion, the differences observed in the homeostasis of the intestinal epithelium of the small versus the large intestines in *Itch*$^{a18H/a18H}$ animals provide physiological insight into regional specificities of these segments of the gastrointestinal tract. Further studies aimed at defining the molecular pathways downstream of ITCH and determining whether the phenotype of the *Itch*$^{a18H/a18H}$ small intestine resembles that of "mucosal healing" in IBD following the abatement of inflammation may allow for the identification of novel biomarkers associated with long-term remission and low risk of surgical treatment in IBD as well as potential new avenues for therapeutic intervention.

Supplementary Material

Refer to Web version on PubMed Central for supplementary material.

Acknowledgments

The authors gratefully acknowledge Dr. Margeaux Wetendorf for initiating the *Itch*$^{a18H/a18H}$ by *Apc*$^{Min/+}$ animal crosses. We thank Ms. Celestia Davis for imparting her expertise in polyp counting, Dr. Bob Price and Mr. Jeff Davis for assistance with transmission electron microscopy, Dr. Hexin Chen for the kind gift of Ki67 antibody, as well as Dr. Jeffery Twiss and Dr. Seung Joon Lee for their invaluable assistance and advice with imaging.

Sources of funding

This work was supported by the National Institutes of Health [P20 RR017698 to L.E.M.], an ASPIRE grant from the Office of the Vice President for Research at the University of South Carolina [L.E.M.], a SPARC Graduate Research Grant from the Office of the Vice President for Research at the University of South Carolina [H.L.M.], and SURF grant from the South Carolina Honors College [A.H.].

Abbreviations

AP	alkaline phosphatase
BrdU	bromodeoxyuridine
CBC	crypt base columnar
EDTA	ethylenediaminetetraacetic acid
EMT	epithelial mesenchymal transition
H & E	hematoxylin and eosin
Hh	hedgehog
IBD	inflammatory bowel disease
IHC	immunohistochemistry
PBS	phosphate buffered saline
SD	standard deviation
SEM	standard error of the mean
TA	transit amplifying

References

Agace WW, McCoy KD. Regionalized development and maintenance of the intestinal adaptive immune landscape. Immunity. 2017; 46:532–548. [PubMed: 28423335]

Barker N. Adult intestinal stem cells: critical drivers of epithelial homeostasis and regeneration. Nat Rev Mol Cell Biol. 2014; 15:19–33. [PubMed: 24326621]

Barker N, van Es JH, Kuipers J, Kujala P, van den Born M, Cozijnsen M, Haegebarth A, Korving J, Begthel H, Peters PJ, Clevers H. Identification of stem cells in small intestine and colon by marker gene Lgr5. Nature. 2007; 449:1003–1007. [PubMed: 17934449]

Basak O, van de Born M, Korving J, Beumer J, van der Elst S, van Es JH, Clevers H. Mapping early fate determination in Lgr5+ crypt stem cells using a novel Ki67-RFP allele. Embo J. 2014; 33:2057–2068. [PubMed: 25092767]

Basheer WA, Harris BS, Mentrup HL, Abreha M, Thames EL, Lea JB, Swing DA, Copeland NG, Jenkins NA, Price RL, Matesic LE. Cardiomyocyte-specific overexpression of the ubiquitin ligase Wwp1 contributes to reduction in Connexin 43 and arrhythmogenesis. J Mol Cell Cardiol. 2015; 88:1–13. [PubMed: 26386426]

Berer K, Mues M, Koutrolos M, Rasbi ZA, Boziki M, Johner C, Wekerle H, Krishnamoorthy G. Commensal microbiota and myelin autoantigen cooperate to trigger autoimmune demyelination. Nature. 2011; 479:538–541. [PubMed: 22031325]

Bischoff SC, Barbara G, Buurman W, Ockhuizen T, Schulzke JD, Serino M, Tilg H, Watson A, Wells JM. Intestinal permeability - a new target for disease prevention and therapy. Bmc Gastroenterol. 2014:14. [PubMed: 24422755]

Brenchley JM, Price DA, Schacker TW, Asher TE, Silvestri G, Rao S, Kazzaz Z, Bornstein E, Lambotte O, Altmann D, Blazar BR, Rodriguez B, Teixeira-Johnson L, Landay A, Martin JN, Hecht FM, Picker LJ, Lederman MM, Deeks SG, Douek DC. Microbial translocation is a cause of systemic immune activation in chronic HIV infection. Nat Med. 2006; 12:1365–1371. [PubMed: 17115046]

Buller NV, Rosekrans SL, Westerlund J, van den Brink GR. Hedgehog signaling and maintenance of homeostasis in the intestinal epithelium. Physiology. 2012; 27:148–155. [PubMed: 22689790]

Burstone MS. Histochemical demonstration of phosphatases in frozen sections with naphthol AS-phosphates. J Histochem Cytochem. 1961; 9:146–153. [PubMed: 13875051]

Cho KR, Vogelstein B. Genetic alterations in the adenoma–carcinoma sequence. Cancer. 1992; 70:1727–1731. [PubMed: 1516027]

Di Marcotullio L, Greco A, Mazza D, Canettieri G, Pietrosanti L, Infante P, Coni S, Moretti M, De Smaele E, Ferretti E, Screpanti I, Gulino A. Numb activates the E3 ligase Itch to control Gli1 function through a novel degradation signal. Oncogene. 2011; 30:65–76. [PubMed: 20818436]

Elphick DA, Mahida YR. Paneth cells: their role in innate immunity and inflammatory disease. Gut. 2005; 54:1802–1809. [PubMed: 16284290]

Foersch S, Neurath MF. Colitis-associated neoplasia: molecular basis and clinical translation. Cell Mol Life Sci. 2014; 71:3523–3535. [PubMed: 24830703]

Garrett WS, Gordon JI, Glimcher LH. Homeostasis and inflammation in the intestine. Cell. 2010; 140:859–870. [PubMed: 20303876]

Gersemann M, Becker S, Kubler I, Koslowski M, Wang G, Herrlinger KR, Griger J, Fritz P, Fellermann K, Schwab M, Wehkamp J, Stange EF. Differences in goblet cell differentiation between Crohn's disease and ulcerative colitis. Differentiation. 2009; 77:84–94. [PubMed: 19281767]

Gregorieff A, Stange DE, Kujala P, Begthel H, van den Born M, Korving J, Peters PJ, Clevers H. The ets-domain transcription factor Spdef promotes maturation of goblet and paneth cells in the intestinal epithelium. Gastroenterology. 2009; 137(1333–1345):e1331–e1333.

Grimelius L. Silver stains demonstrating neuroendocrine cells. Biotech Histochem. 2004; 79:37–44. [PubMed: 15223752]

Gunther C, Martini E, Wittkopf N, Amann K, Weigmann B, Neumann H, Waldner MJ, Hedrick SM, Tenzer S, Neurath MF, Becker C. Caspase-8 regulates TNF-alpha-induced epithelial necroptosis and terminal ileitis. Nature. 2011; 477:335–339. [PubMed: 21921917]

Halbleib JM, Nelson WJ. Cadherins in development: cell adhesion, sorting, and tissue morphogenesis. Gene Dev. 2006; 20:3199–3214. [PubMed: 17158740]

Hermiston ML, Wong MH, Gordon JI. Forced expression of E-cadherin in the mouse intestinal epithelium slows cell migration and provides evidence for nonautonomous regulation of cell fate in a self-renewing system. Gene Dev. 1996; 10:985–996. [PubMed: 8608945]

Hustad CM, Perry WL, Siracusa LD, Rasberry C, Cobb L, Cattanach BM, Kovatch R, Copeland NG, Jenkins NA. Molecular-genetic characterization of 6 recessive viable alleles of the mouse agouti locus. Genetics. 1995; 140:255–265. [PubMed: 7635290]

Jin HS, Park Y, Elly C, Liu YC. Itch expression by Treg cells controls Th2 inflammatory responses. J Clin Investig. 2013; 123:4923–4934. [PubMed: 24135136]

Johansson ME, Hansson GC. Immunological aspects of intestinal mucus and mucins. Nat Rev Immunol. 2016; 16:639–649. [PubMed: 27498766]

Kathania M, Khare P, Zeng M, Cantarel B, Zhang H, Ueno H, Venuprasad K. Itch inhibits IL-17-mediated colon inflammation and tumorigenesis by ROR-gammat ubiquitination. Nat Immunol. 2016; 17:997–1004. [PubMed: 27322655]

Lee YK, Menezes JS, Umesaki Y, Mazmanian SK. Proinflammatory T-cell responses to gut microbiota promote experimental autoimmune encephalomyelitis. Proc Natl Acad Sci USA. 2011; 108(Suppl 1):4615–4622. [PubMed: 20660719]

Lohr NJ, Molleston JP, Strauss KA, Torres-Martinez W, Sherman EA, Squires RH, Rider NL, Chikwava KR, Cummings OW, Morton DH, Pufienberger EG. Human ITCH E3 ubiquitin ligase deficiency causes syndromic multisystem autoimmune disease. Am J Hum Genet. 2010; 86:447–453. [PubMed: 20170897]

Mankertz J, Schulzke JD. Altered permeability in inflammatory bowel disease: pathophysiology and clinical implications. Curr Opin Gastroenterol. 2007; 23:379–383. [PubMed: 17545772]

Mukherjee S, Vaishnava S, Hooper LV. Multi-layered regulation of intestinal antimicrobial defense. Cell Mol Life Sci. 2008; 65:3019–3027. [PubMed: 18560756]

Nalbantoglu I, Blanc V, Davidson NO. Characterization of colorectal cancer development in Apc (min/+) mice. Methods Mol Biol. 2016; 1422:309–327. [PubMed: 27246043]

Nenci A, Becker C, Wullaert A, Gareus R, van Loo G, Danese S, Huth M, Nikolaev A, Neufert C, Madison B, Gumucio D, Neurath MF, Pasparakis M. Epithelial NEMO links innate immunity to chronic intestinal inflammation. Nature. 2007; 446:557–561. [PubMed: 17361131]

Okumura R, Takeda K. Roles of intestinal epithelial cells in the maintenance of gut homeostasis. Exp Mol Med. 2017; 49:e338. [PubMed: 28546564]

Parker A, Maclaren OJ, Fletcher AG, Muraro D, Kreuzaler PA, Byrne HM, Maini PK, Watson AJM, Pin C. Cell proliferation within small intestinal crypts is the principal driving force for cell migration on villi. Faseb J. 2017; 31:636–649. [PubMed: 27811059]

Parravicini V, Field AC, Tomlinson PD, Basson MA, Zamoyska R. Itch−/−alphabeta and gammadelta T cells independently contribute to autoimmunity in Itchy mice. Blood. 2008; 111:4273–7282. [PubMed: 18256323]

Peglion F, Llense F, Etienne-Manneville S. Adherens junction treadmilling during collective migration. Nat Cell Biol. 2014; 16:639. [PubMed: 24929360]

Pellettieri J, Sanchez Alvarado A. Cell turnover and adult tissue homeostasis: from humans to planarians. Annu Rev Genet. 2007; 41:83–105. [PubMed: 18076325]

Perry WL, Hustad CM, Swing DA, O'Sullivan TN, Jenkins NA, Copeland NG. The itchy locus encodes a novel ubiquitin protein ligase that is disrupted in a18H mice. Nat Genet. 1998; 18:143–146. [PubMed: 9462742]

Popovic D, Vucic D, Dikic I. Ubiquitination in disease pathogenesis and treatment. Nat Med. 2014; 20:1242–1253. [PubMed: 25375928]

Powell DW, Pinchuk IV, Saada JI, Chen X, Mifflin RC. Mesenchymal cells of the intestinal lamina propria. Annu Rev Physiol. 2011; 73:213–237. [PubMed: 21054163]

Ramon HE, Riling CR, Bradfield J, Yang B, Hakonarson H, Oliver PM. The ubiquitin ligase adaptor Ndfip1 regulates T cell-mediated gastrointestinal inflammation and inflammatory bowel disease susceptibility. Mucosal Immunol. 2011; 4:314–324. [PubMed: 20962770]

Sandler NG, Koh C, Roque A, Eccleston JL, Siegel RB, Demino M, Kleiner DE, Deeks SG, Liang TJ, Heller T, Douek DC. Host response to translocated microbial products predicts outcomes of patients with HBV or HCV infection. Gastroenterology. 2011; 141:1220–1230. e1221–e1223. (1230). [PubMed: 21726511]

Sansom OJ, Mansergh FC, Evans MJ, Wilkins JA, Clarke AR. Deficiency of SPARC suppresses intestinal tumorigenesis in APCMin/+ mice. Gut. 2007; 56:1410–1414. [PubMed: 17299058]

Schenk M, Mueller C. The mucosal immune system at the gastrointestinal barrier. Best Pract Res Clin Gastroenterol. 2008; 22:391–409. [PubMed: 18492562]

Schneider MR, Dahlhoff M, Horst D, Hirschi B, Trulzsch K, Muller-Hocker J, Vogelmann R, Allgauer M, Gerhard M, Steininger S, Wolf E, Kolligs FT. A key role for E-cadherin in intestinal homeostasis and Paneth cell maturation. PLoS One. 2010; 5:e14325. [PubMed: 21179475]

Strikoudis A, Guillamot M, Aifantis I. Regulation of stem cell function by protein ubiquitylation. EMBO Rep. 2014; 15:365–382. [PubMed: 24652853]

Tao MF, Scacheri PC, Marinis JM, Harhaj EW, Matesic LE, Abbott DW. ITCH K63-ubiquitinates the NOD2 binding protein, RIP2, to influence inflammatory signaling pathways. Curr Biol. 2009; 19:1255–1263. [PubMed: 19592251]

Theivanthiran B, Kathania M, Zeng M, Anguiano E, Basrur V, Vandergriff T, Pascual V, Wei WZ, Massoumi R, Venuprasad K. The E3 ubiquitin ligase Itch inhibits p38alpha signaling and skin inflammation through the ubiquitylation of Table 1. Sci Signal. 2015; 8:ra22. [PubMed: 25714464]

Tucker JM, Davis C, Kitchens ME, Bunni MA, Priest DG, Spencer HT, Berger FG. Response to 5-fluorouracil chemotherapy is modified by dietary folic acid deficiency in Apc(Min/+) mice. Cancer Lett. 2002; 187:153–162. [PubMed: 12359363]

Tucker JM, Murphy JT, Kisiel N, Diegelman P, Barbour KW, Davis C, Medda M, Alhonen L, Janne J, Kramer DL, Porter CW, Berger FG. Potent modulation of intestinal tumorigenesis in Apcmin/+ mice by the polyamine catabolic enzyme spermidine/spermine N1-acetyltransferase. Cancer Res. 2005; 65:5390–5398. [PubMed: 15958588]

Turner JR. Intestinal mucosal barrier function in health and disease. Nat Rev Immunol. 2009; 9:799–809. [PubMed: 19855405]

Vaishnava S, Behrendt CL, Ismail AS, Eckmann L, Hooper LV. Paneth cells directly sense gut commensals and maintain homeostasis at the intestinal host-microbial interface. Proc Natl Acad Sci USA. 2008; 105:20858–20863. [PubMed: 19075245]

van der Flier LG, Clevers H. Stem cells, self-renewal, and differentiation in the intestinal epithelium. Annu Rev Physiol. 2009; 71:241–260. [PubMed: 18808327]

van der Gracht E, Zahner S, Kronenberg M. When insult is added to injury: cross talk between ILCs and intestinal epithelium in IBD. Mediat Inflamm. 2016; 2016:9765238.

Vlantis K, Wullaert A, Sasaki Y, Schmidt-Supprian M, Rajewsky K, Roskams T, Pasparakis M. Constitutive IKK2 activation in intestinal epithelial cells induces intestinal tumors in mice. J Clin Investig. 2011; 121:2781–2793. [PubMed: 21701067]

Wehkamp J, Koslowski M, Wang G, Stange EF. Barrier dysfunction due to distinct defensin deficiencies in small intestinal and colonic Crohn's disease. Mucosal Immunol. 2008; 1(Suppl 1):S67–S74. [PubMed: 19079235]

Welz PS, Wullaert A, Vlantis K, Kondylis V, Fernandez-Majada V, Ermolaeva M, Kirsch P, Sterner-Kock A, van Loo G, Pasparakis M. FADD prevents RIP3-mediated epithelial cell necrosis and chronic intestinal inflammation. Nature. 2011; 477:330–334. [PubMed: 21804564]

Wen L, Ley RE, Volchkov PY, Stranges PB, Avanesyan L, Stonebraker AC, Hu C, Wong FS, Szot GL, Bluestone JA, Gordon JI, Chervonsky AV. Innate immunity and intestinal microbiota in the development of Type 1 diabetes. Nature. 2008; 455:1109–1113. [PubMed: 18806780]

Williams JM, Duckworth CA, Burkitt MD, Watson AJ, Campbell BJ, Pritchard DM. Epithelial cell shedding and barrier function: a matter of life and death at the small intestinal villus tip. Vet Pathol. 2015; 52:445–455. [PubMed: 25428410]

Wong MH, Hermiston ML, Syder AJ, Gordon JI. Forced expression of the tumor suppressor adenomatosis polyposis coli protein induces disordered cell migration in the intestinal epithelium. Proc Natl Acad Sci USA. 1996; 93:9588–9593. [PubMed: 8790374]

Wu HJ, Ivanov II, Darce J, Hattori K, Shima T, Umesaki Y, Littman DR, Benoist C, Mathis D. Gut-residing segmented filamentous bacteria drive autoimmune arthritis via T helper 17 cells. Immunity. 2010; 32:815–827. [PubMed: 20620945]

Appendix A. Supplementary material

Supplementary data associated with this article can be found in the online version at doi: 10.1016/j.diff.2017.12.003.

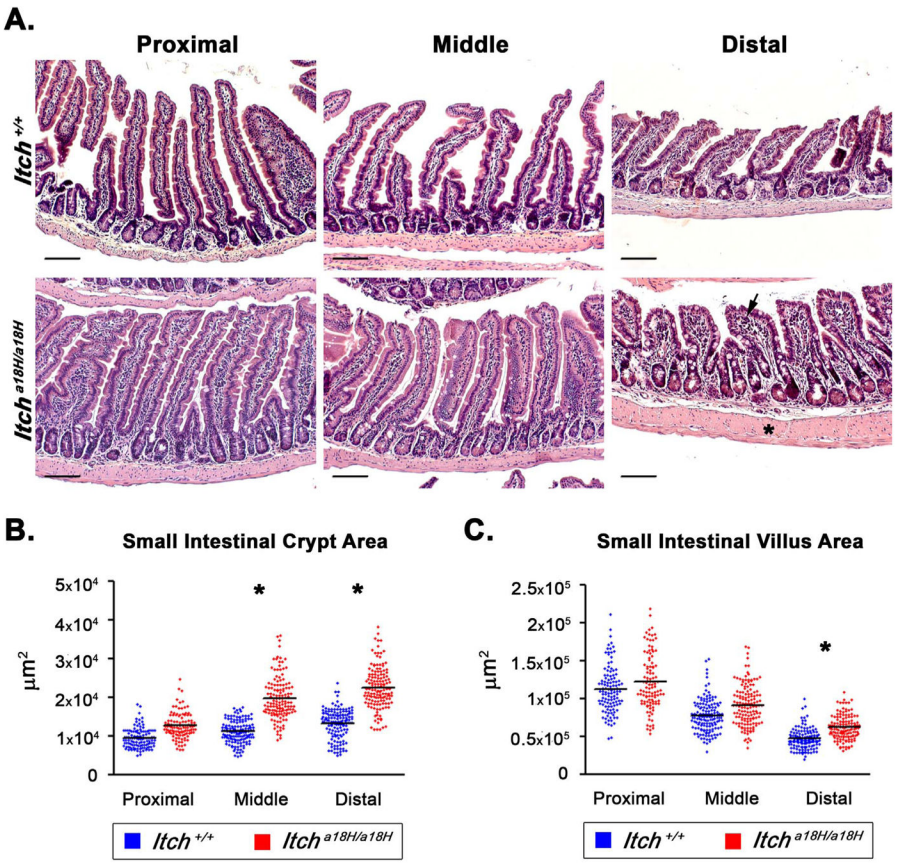

Fig. 1.

Small intestinal architecture is altered in *Itch*$^{a18H/a18H}$ animals. (A) Representative H & E stained paraffin-embedded small intestinal sections derived from the proximal (left most column), middle (center column), and distal (right hand column) segments of young adult *Itch*$^{+/+}$ and *Itch*$^{a18H/a18H}$ animals accentuate an enlargement of the intestinal crypt, villus blunting with crowding of epithelial cells, and thickening of the muscularis propria (asterisk) in *Itch*$^{a18H/a18H}$ animals, becoming more pronounced distally. Mild inflammation was also occasionally noted in the lamina propria (arrow). Scale bars = 200 µm. (B) Small intestinal crypt and villus areas from young adult *Itch*$^{+/+}$ (n = 4 or 5) and *Itch*$^{a18H/a18H}$ (n = 5) were measured in µm^2 using ImageJ. A minimum of 25 well-orientated crypts or villi from at least seven different 10x fields were measured per animal. Average crypt area was significantly increased (*$p < 0.005$) in the middle and distal small intestine of *Itch*$^{a18H/a18H}$ compared to *Itch*$^{+/+}$. (C) Average villus area was significantly increased (*$p < 0.05$) distally in the small intestine of *Itch*$^{a18H/a18H}$ animals compared to *Itch*$^{+/+}$.

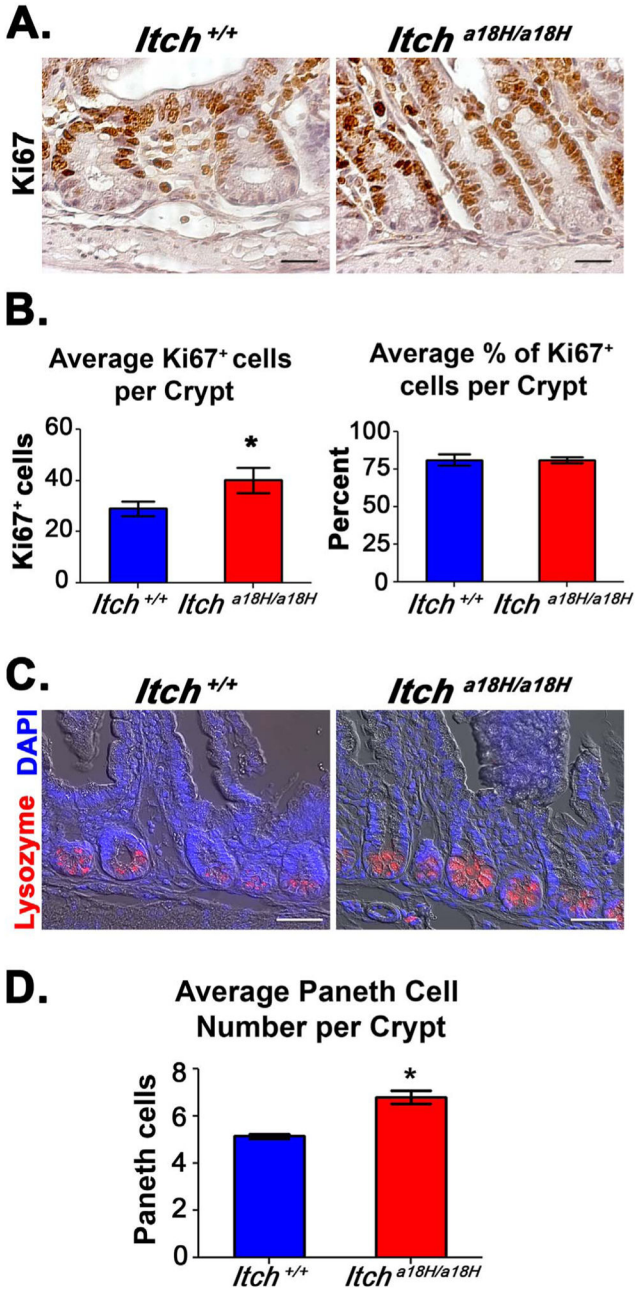

Fig. 2.

Crypt expansion in *Itch*$^{a18H/a18H}$ animals is accompanied by an increase in proliferating TA cells and differentiated Paneth cells. (A) Pictured are representative micrographs of IHC performed on paraffin-embedded distal intestinal sections derived from young adult *Itch*$^{+/+}$ and *Itch*$^{a18H/a18H}$ animals (n = 5 for each genotype) using an anti-Ki67 antibody and subsequently counterstained with hematoxylin. Animals lacking ITCH appear to have increased cellular proliferation in the crypt. Scale bars = 50 μm. (B) Average number and average percentage of Ki67^{+} cells in the crypts from adult *Itch*$^{+/+}$ (n = 5) and *Itch*$^{a18H/a18H}$ (n = 5) animals. Ki67^{+} cells and total cell numbers were counted from 25 well-oriented

crypts in a minimum of nine different 20x fields per animal. *Itch*$^{a18H/a18H}$ animals had, on average, 13 more Ki67^{+} cells per crypt which was statistically significant (*$p < 0.01$). No difference was observed in the percentage of proliferating cells within the crypt. Error bars represent SD. (C) Representative phase contrast-coupled immunofluorescent images of paraffin-embedded sections of distal intestine from five adult *Itch*$^{+/+}$ and five age-matched *Itch*$^{a18H/a18H}$ animals stained with anti-lysozyme (red) and counterstained with DAPI (blue) to detect nuclei. Scale bars = 100 μm. (D) Average number of Paneth cells per crypt from adult *Itch*$^{+/+}$ (n = 5) and *Itch*$^{a18H/a18H}$ (n = 5) animals. Paneth cell numbers from 30 crypts in a minimum of 12 different 20x fields were averaged to determine that *Itch*$^{a18H/a18H}$ animals have significantly more Paneth cells (*$p < 0.05$) than *Itch*$^{+/+}$ animals. Error bars represent SEM (For interpretation of the references to color in this figure legend, the reader is referred to the web version of this article.).

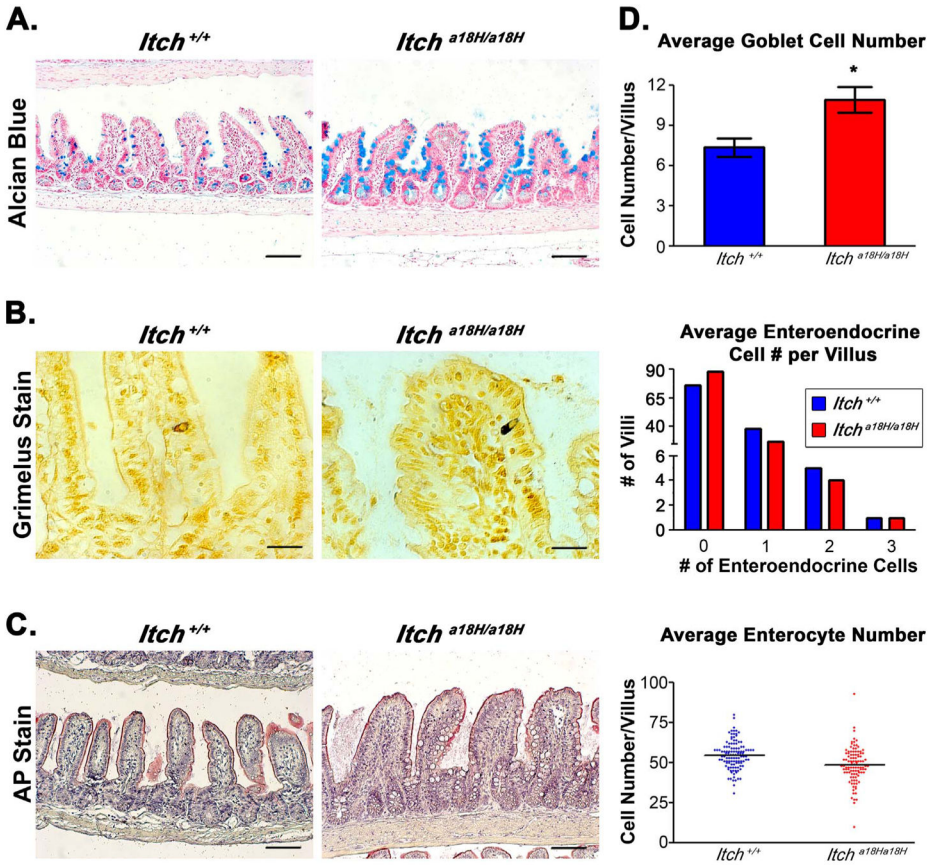

Fig. 3.

Loss of ITCH promotes goblet cell differentiation. (A) Paraffin-embedded intestinal sections stained with alcian blue, pH 2.5 and counterstained with nuclear fast red distinguish goblet cells from adult *Itch*$^{+/+}$ and *Itch*$^{a18H/a18H}$ animals. Scale bars = 200 μm. (B) Pictured are representative *Itch*$^{+/+}$ and *Itch*$^{a18H/a18H}$ derived paraffin-embedded sections stained with 1% silver nitrate to identify enteroendocrine cells in the small intestine. Scale bars = 200 μm. (C) Paraffin-embedded sections stained with AP highlights the brush boarder of enterocytes on the villi of *Itch*$^{+/+}$ and *Itch*$^{a18H/a18H}$ animals. Scale bars = 200 μm. (D) Average number of goblet cells, enteroendocrine cells, and enterocytes located on the villus of *Itch*$^{+/+}$ (n = 4) and *Itch*$^{a18H/a18H}$ (n = 4) animals. Indicated type of cells were counted on 30 villus structures from a minimum of eight different 10x fields per animal. Enteroendocrine cell counts are presented as a histogram of the total number of villus structures bearing no, one, two or three cells in *Itch*$^{+/+}$ (n = 4) and *Itch*$^{a18H/a18H}$ (n = 4) animals. *Itch*$^{a18H/a18H}$ animals have a statistically significant increase (*****$p < 0.05$) in goblet cells. There was no statistically significant difference in enteroendocrine or enterocyte cell number. Error bars represent SEM for goblet cell counts.

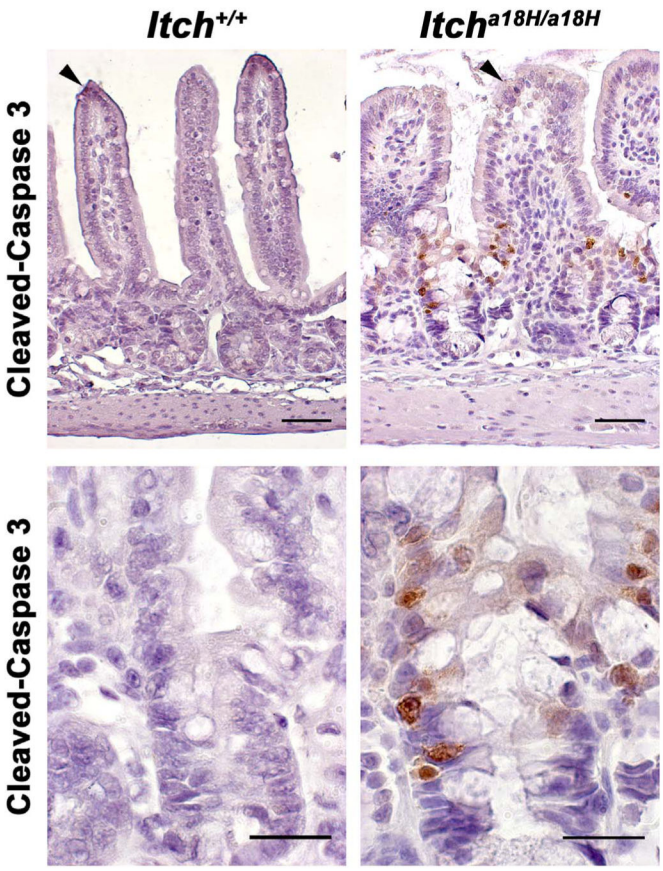

Fig. 4.

Loss of ITCH promotes epithelial apoptosis in the small intestine. Paraffin embedded sections from the distal small intestine of young adult *Itch*$^{+/+}$ and *Itch*$^{a18H/a18H}$ animals (n = 4 for each genotype) were immunostained for cleaved-caspase 3 and counterstained with hematoxylin. Representative photomicrographs are shown. While rare apoptotic cells could be found at the tips of villi in animals of both genotypes (arrowheads, top row of micrographs), increased apoptosis was seen at the crypt-villus junction in only those animals lacking ITCH (bottom row, 63x). Scale bars = 100 μm (top row) or 50 μm (bottom row).

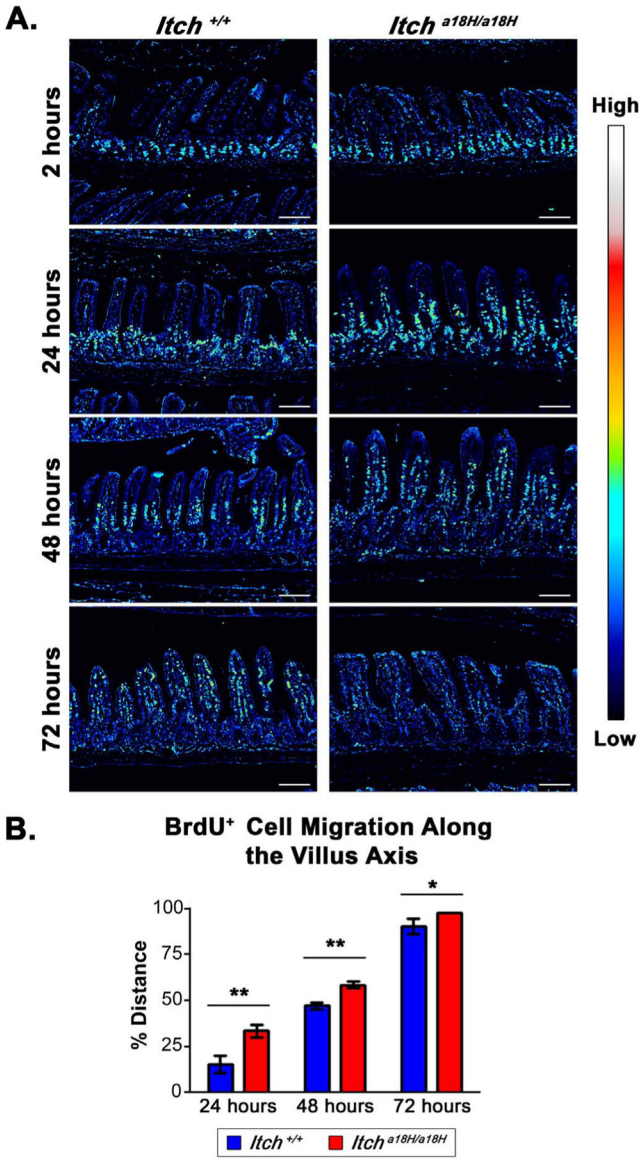

Fig. 5.

Epithelial turnover is increased in animals that lack ITCH. (A) IHC with an anti-BrdU antibody was conducted on paraffin-embedded sections obtained from young adult *Itch*$^{+/+}$ and *Itch*$^{a18H/a18H}$ animals intraperitoneally injected with 100 mg/kg of BrdU. Brightfield images were taken 2, 24, 48, and 72 h post injection and representative examples from each genotype and time point were converted to spectral images using the royal look-up table available in ImageJ. An intensity scale for this spectrum is pictured to the right. These images demonstrate enhanced migration of epithelial cells in *Itch*$^{a18H/a18H}$ animals with complete sloughing by 72 h following the BrdU pulse. Scale bars = 200 μm. (B) Average cell migration of BrdU-labeled cells along the villus axis in *Itch*$^{+/+}$ (n = 3) and *Itch*$^{a18H/a18H}$ (n = 3) animals at 24, 48, and 72 h after BrdU incorporation was calculated by dividing the measured distance of the furthest migrated labeled cell from the base of the villus by the entire length of the villus from 25 villi in a minimum of five different 10x fields per animal.

Since all cells were localized to the crypt in both genotypes at the 2 h timepoint, this data point is not shown. A statistically significant increase in cell migration at was detected in *Itch*$^{a18H/a18H}$ derived tissues at 24 (**$p < 0.005$), 48 (**$p < 0.005$), and 72 h (*$p < 0.05$) versus tissues derived from *Itch*$^{+/+}$ animals. Error bars represent SD.

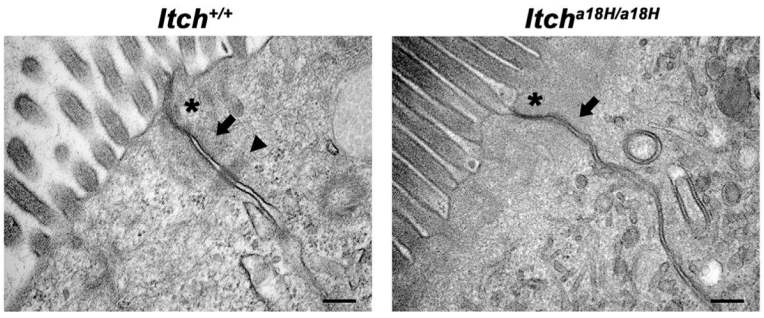

Fig. 6.

Itch$^{a18H/a18H}$ animals have altered cell-cell junctions. Representative transmission electron micrographs of cell-cell junctions (tight junctions marked by asterisks, adherens junctions by arrows, and desmosomes by arrow head) from the proximal small intestine of nine week-old *Itch*$^{+/+}$ and *Itch*$^{a18H/a18H}$ animals are depicted here. In total samples from four animals of each genotype were examined. *Itch*$^{a18H/a18H}$ animals lack identifiable desmosomes and adherens junctions appeared more disorganized than the ITCH sufficient control samples. Scale bar = 200 nm.

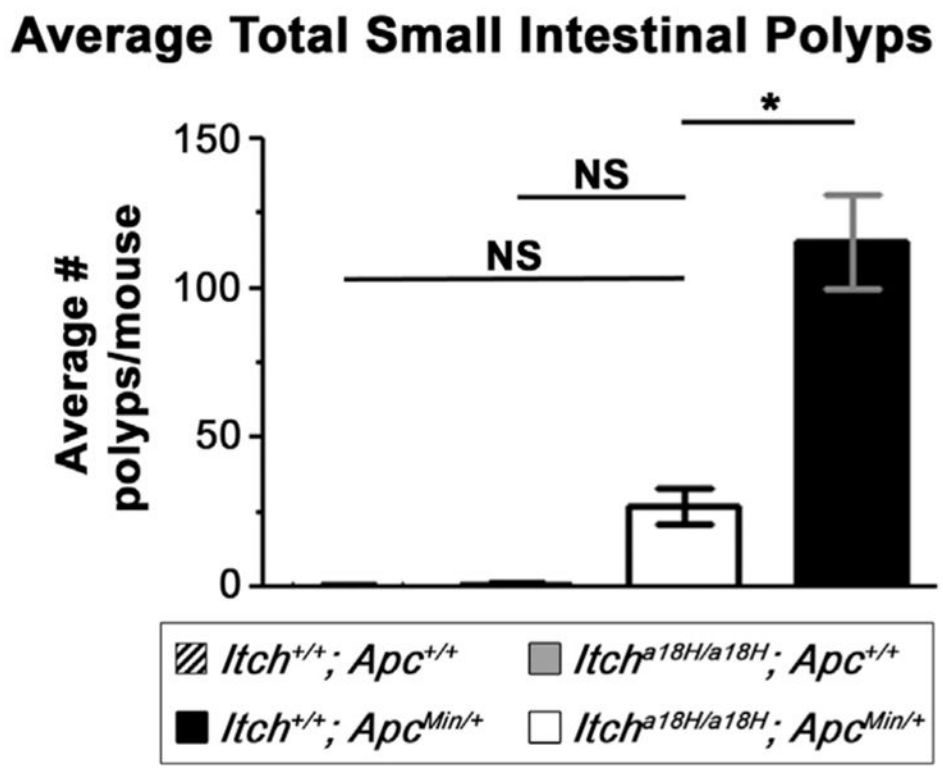

Fig. 7.

Loss of ITCH is protective in $Apc^{Min/+}$-induced tumorigenesis. Polyps from the small intestine of 15 week-old $Itch^{+/+}$; $Apc^{+/+}$ (n = 11), $Itch^{a18H/a18H}$; $Apc^{+/+}$ (n = 11), $Itch^{+/+}$; $Apc^{Min/+}$ (n = 11), and $Itch^{a18H/a18H}$; $Apc^{Min/+}$ (n = 11) animals were visualized by staining the flushed and fixed small intestine with 0.1% methylene blue. Polyps from the entire length of the intestine were counted under a dissecting microscope. The graph shown here depicts the average number of small intestinal polyps per animal. $Itch^{a18H/a18H}$; $Apc^{Min/+}$ animals were observed to have a significant reduction in tumor burden compared to $Itch^{+/+}$; $Apc^{Min/+}$ littermates (*$p < 0.001$, NS = not significant). Error bars represent SD.